THE JOURNAL OF PHYSICAL CHEMISTRY B

Article

pubs.acs.org/JPCB

Building a Model of the Blue Cone Pigment Based on the Wild Type Rhodopsin Structure with QM/MM Methods

Jan S. Frähmcke,[†] Marius Wanko,[‡] and Marcus Elstner*[,†,§]

[†]Institute for Physical and Theoretical Chemistry, TU Braunschweig, Hans-Sommer-Strasse 10, D-38106 Braunschweig, Germany

[‡]Nano-Bio Spectroscopy Group and ETSF Scientific Development Centre, Departamento de Física de Materiales, Universidad del País Vasco, Centro de Física de Materiales CSIC-UPV/EHU, Av. Tolosa 72, E-20018 San Sebastián, Spain

[§]Institute of Physical Chemistry, Karlsruhe Institute of Technology, Kaiserstrasse 12, D-76131 Karlsruhe, Germany

Supporting Information

ABSTRACT: Understanding the mechanism of color tuning of the retinal chromophore by its host protein became one of the key issues in the research on rhodopsins. While early mutation studies addressed its genetic origin, recent studies advanced to investigate its structural origin, based on X-ray crystallographic structures. For the human cone pigments, no crystal structures have been produced, and homology models were employed to elucidate the origin of its blue-shifted absorption. In this theoretical study, we take a different route to establish a structural model for human blue. Starting from the well-resolved structure of bovine rhodopsin, we derive multiple mutant models by stepwise mutation and equilibration using molecular dynamics simulations in a hybrid quantum mechanics/molecular mechanics framework. Our 30fold mutant reproduces the experimental UV−vis absorption shift of 0.45 eV and provides new insights about both structural and genetic factors that affect the excitation energy. Electrostatic effects of individual amino acids and collaborative structural effects are analyzed using semiempirical (OM2/MRCI) and ab initio (SORCI) multireference approaches.

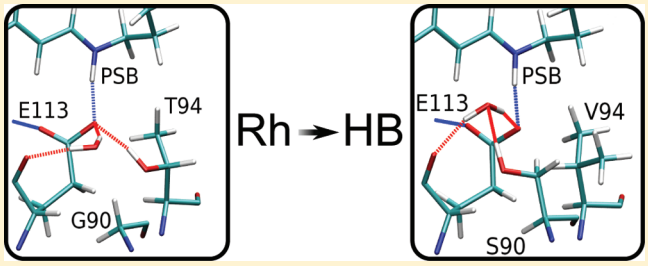

INTRODUCTION

Retinal proteins are involved in several biochemical processes, such as vision (e.g., rhodopsin, rod pigments), bioenergetics [bacteriorhodopsin (bR)], phototaxis [pharaonis sensory rhodopsin (ppR)], and ion transport (channel rhodopsins). They all consist of seven transmembrane helices (opsin) and a retinal chromophore, which is covalently bound to a lysine residue via a protonated Schiff base (PSB). The PSB of retinal forms a light-absorbing polyene of six conjugated double bonds, terminated by a β-ionone ring.

The human retina has two cell types for light detection, the rod cells for dim-light vision, containing rhodopsin (Rh) with the retinal in 11-*cis* configuration absorbing at 498 nm (2.49 eV),[1] and three classes of cone cells, containing the human red (HR) (2.21 eV, 560 nm),[2] green (HG) (2.33 eV, 530 nm),[2] and blue (HB) (2.91−2.99 eV, 414−426 nm)[2−4] pigments.

Several factors have been shown to be important for color tuning in retinal proteins, namely, the retinal twist, the hydrogen-bonding interaction of retinal with the counterion, and the electrostatic interaction of retinal with the opsin. For the cone pigments, this has been studied in some detail both experimentally, by the groups of Mathies and Sakmar,[5−7] and in theoretical studies[8−12] based on a homology model structure.[13]

Although there are high-resolution X-ray structures available for several retinal proteins, like bR, Rh, and others, this is not the case for HR, HG, and HB, where only homology models are available (PDB codes 1KPX, 1KPW, 1KPN). Stenkamp et al.[13] modeled the HB opsin structure by aligning the primary structure of wild type (WT) Rh and HB opsin and mapping the amino acids to the known structure of WT Rh (1HZX[14]). The retinal molecule was then inserted into the three-dimensional structure, and the binding pocket was geometry-optimized. The resulting homology model of HB (PDB code 1KPN) was used in three recent studies[8,11,12] that investigated the mechanism of color tuning.

Homology modeling is a powerful tool if there is a high sequence similarity to a protein with known structure. However, HB and Rh are identical to only 41%.[13] To be more specific, only 20 of the 43 amino acids close to retinal (within 5 Å) are conserved (only 28 of 61 amino acids within 6 Å). This situation multiplies the difficulties that normally arise in homology modeling, namely, the structural uncertainties in rotamer states and proper solvation, i.e., placement of protein internal water molecules. Before using homology models in theoretical studies, these uncertainties should be eliminated, as calculated properties can be strongly affected.

Specifically, in the case of the 1KPN model for HB, we observe the following issues that might affect the calculation of excitation energies: The side chains of amino acids Thr118 and Ser186 seem to have the wrong orientation. The study of

Received: September 7, 2011
Revised: February 13, 2012
Published: February 14, 2012

Fujimoto et al.[11] ascribes a major part of the RH−HB shift to these residues. The OH group of Thr118 is rotated by 120°, and that of Tyr10 is translocated by ca. 9 Å compared with Rh. Due to missing water molecules and cofactor during the modeling process, the hydrogen-bonding pattern can be disturbed, affecting even conserved residues. Ser186, e.g., is rotated in 1KPN to form a hydrogen bond with Glu113, whereas in the Rh structures 1HZX and 1U19 it forms a hydrogen bond to Wat2a.

In principle, these problems can be resolved by performing sufficiently long MD simulations and using advanced sampling techniques. In the present case, it is not clear if the required time scales can be achieved in classical MM MD simulations. Classical force fields, however, are not accurate enough to reliably predict rotamer occupations. Moreover, it has been pointed out that conventional force fields have problems in describing strongly hydrogen-bonded networks,[15−17] which in the case of bR results in an instable retinal binding site.[15] Similar problems should be expected also for HB. Therefore, it is desirable to perform MD at the QM/MM level and to investigate rotamers and cavities for water, individually.

As a complement to the homology modeling procedure, we decided to start from the WT Rh crystal structure and mutate the residues in the binding pocket step-by-step to those in HB, thereby analyzing the rotamer states one by one using the QM/MM simulations. This is very similar to the procedure of Lin et al., who experimentally investigated a 12-fold Rh mutant.[6] These experiments provide valuable benchmark data for our procedure. Remaining important residues for the color shift are determined using a perturbational approach. By carefully testing all rotamers in short MD simulations, we arrive at a model that does not deviate from the known X-ray structures due to artificial rotations.

METHODS

QM/MM with SCC-DFTB. We used hybrid quantum mechanics/molecular mechanics (QM/MM) schemes[18−21] to generate structures and calculate excitation energies. Apart from calculating excitation energies, a QM description of the chromophore is necessary because of the lack of an accurate MM method.

We used the CHARMM27[22] force field for the MM part, and the QM method of choice is SCC-DFTB,[23] which is about 3 orders of magnitude faster than DFT methods, while describing the properties of the chromophore with comparable accuracy.[24] The SCC-DFTB/CHARMM[25] implementation has been widely documented elsewhere.[26,27] In this work, SCC-DFTB with third-order terms in charge-density fluctuations has been used, as described by Yang et al.[28]

If not noted differently, we used a QM region consisting of retinal and the complex counterion. This region is called QM4 because four residues are included (Lys296, Glu113, Thr94, and Wat2b). Note that the number of QM4 atoms can change in mutants, e.g., from 85 atoms in WT Rh to 87 in the 24fold mutant. Calculations with QM4 allow for charge exchange between the chromophore and the complex counterion, which can affect excitation energies. We tested the convergence of this charge transfer with the size of the QM region and found it converged for QM4 (see Supporting Information). In special cases, other QM regions were used: QM1 (Lys296, 63 atoms), QM2 (Lys296 and Glu113, 73 atoms), and QM5_90 (QM4 and Ser90, G90S mutant: 91 atoms, 24fold mutant: 93 atoms). The QM/MM boundary was always chosen to be between the C_α and C_β bond. The valence of the QM fragment was then saturated with a hydrogen link atom. The QM/MM frontier was treated using the *divided frontier* (DIV) scheme.[29] MD simulations were carried out with the SCC-DFTB/CHARMM setup to test the stability of all models using a time step of 1 fs. After heating to 300 K and equilibration, the Nosé−Hoover thermostat[30,31] was employed for simulation times of 500 ps.

Excited States. Excitation energies were calculated with two different multireference CI methods. We used the fast semiempirical OM2/MRCI included in the MNDO99 program package[32,33] for the search of important mutations that have an impact on the excitation energy. In this procedure, we switched off the side chain partial charges of all amino acids successively and calculated the shift in excitation energy. This method works without structural relaxation of the model structure and is called perturbation analysis. OM2/MRCI has been benchmarked for calculating shifts in excitation energies of retinal and well reproduces results of higher level methods, such as CASPT2 and SORCI.[24]

The second method to calculate excitation energies is the quantum mechanical *Spectroscopy ORiented Configuration Interaction* (SORCI) method,[34] implemented in the ORCA quantum chemical package.[35] SORCI combines the concepts of classical multireference configuration interaction and multireference perturbation theory. All 12 π orbitals were included in the references of the preliminary MRDDCI2 and final MRDDCI3 steps. We used Ahlrich's SV(P) basis set[36] and added diffuse s- and p-functions on the carboxylate oxygens of Glu113 to improve the charge equilibrium between this anionic fragment and the chromophore (see Supporting Information).

To check if the electrostatic representation of the protein has to be improved by including polarization effects, we replaced the CHARMM27 point charges by the explicitly polarized polar.h model, which has been benchmarked for peptides and applied to various rhodopsins.[37−40] For Rh and its mutants, we find absolute excitation energies red-shifted by ca. 0.09 eV, whereas the effect is negligible for the mutation shifts (see Supporting Information). We therefore omit a discussion of protein polarizability in the article and only show results obtained with CHARMM27 point charges for consistency.

Our method (SCC-DFTB/CHARMM for optimization and OM2/MRCI and SORCI for excitation energies) has been successfully applied in a study of the spectral tuning in archaeal rhodopsins and their mutants.[41]

System Setup. The system setup is the same as in our previous work (see details therein).[39] The coordinates of the heavy atoms of WT Rh were obtained from the newest X-ray structure[42] (PDB code: 1U19). This is the best resolved structure with a resolution of 2.2 Å and more water molecules than other available structures (1F88,[43] 1HZX,[14] 1L9H,[44] 1GZM,[45] 2J4Y[46]). There are no crystal structures available for HB and also none for single or multiple mutants.

Standard protonation states were assumed for all titratable amino acids (including Glu181) except Asp83 and Glu122, which are modeled neutral as proposed by experiments and calculations.[39,47] The screening effect of bulk solvent on charged amino acids was included based on the solution of the Poisson−Boltzmann equation according to the charge scaling scheme proposed by Dinner et al.[48] To preserve the outer shape of the protein in the absence of bulk solvent, non-hydrogen atoms with a distance greater than 15 Å to the chromophore were harmonically restrained to their position in the crystal structure during geometry optimization and MD simulations. The force

constants are derived from the B-factors (see Supporting Information).[41] Hydrogen atoms were not constrained.

Single Mutation Models. As a first step, we investigate the effect of single mutations on the structure and excitation energies. Starting from the bovine Rh crystal structure 1U19, we mutated amino acids individually to the corresponding ones in the HB sequence. A simple QM/MM structure optimization may only lead to the next local minimum; therefore we performed QM/MM MD simulations to probe the stability and eventually locate other side chain conformations. Since the time scale of the MD simulations is limited, we also investigated other rotamers not found during the MD by manually changing the orientation of the mutated residue and repeating the QM/MM geometry optimization and MD simulation. This procedure creates a set of residue conformations, which can be discriminated on the basis of their total energy. Of course, the free energy would be a more appropriate measure, but we expect no large entropy contributions because of the highly constrained nature of these conformations, as has been reported, e.g., in our previous study on Rh.[39] Substituting large side chains by smaller ones may introduce a cavity that can be occupied by one or more water molecules. Again, the sophisticated approach would be to perform grand canonical simulations to determine the location of additional water molecules. Since this is very tedious, we decided to place additional water molecules and investigated the resulting H-bonded structure by performing MD simulations. Interestingly, this procedure led to an easy evaluation of the stability of the HBN in all cases, which was stable only when inserting a particular number of water molecules. Otherwise, it would exhibit large fluctuations, or H-bonds would disrupt, as they are not formed in a stable fashion. Note that all models were evaluated by computing excited-state energies. Often, the excitation energies are already a good measure for the reasonability of the structural models, as we have found in our recent work on bR and Rh.[39,40]

Multiple Mutation Models. Multiple mutants were built from the structures of the single mutations, as described above, and then combined into increasingly complex models of the active site. This procedure leads to a large set of structures, as sometimes several conformations of a residue have to be taken into account and have been evaluated by their total energy. Following the procedure described above, repeated geometry optimizations and MD simulations were performed.

Residue Selection. To determine which additional nonconserved amino acids have a sizable impact on the excitation energy, we performed two types of calculations: In a first step, we performed a so-called perturbation analysis for all amino acids, where the partial charges of every residue are deleted to mimic the effect of a mutation into glycine. We have performed the same analysis before to examine the color shift between bR and ppR.[41] This is done without geometry relaxation, and excitation energies are calculated with OM2/MRCI. The electrostatic effect of residue I in structure X is then defined by

$$ES^{X}(I) = \Delta E_{S_1 \leftarrow S_0}(X) - \Delta E_{S_1 \leftarrow S_0}(X \text{ w/o charges of } I) \quad (1)$$

Residues that have an electrostatic effect of $|ES^{WT\ Rh}(I)| \geq 0.004$ eV and are different in the WT Rh and blue cone primary sequence are then modeled as single mutants and included in the multiple mutant. In the second step, we searched the primary structure for further differences, and all mutations in a region of 5 Å around retinal and the Lys296 side chain were modeled as single mutants and included in the multiple mutant.

In the following, we will use the numbering system of WT Rh for the protein and the numbering of water molecules from the crystal structure (1U19). For waters Wat2a and Wat2b, which are part of the HBN around Glu181, Ser186, and the complex counterion (Glu113, Thr94, Wat2b), respectively, we use the special names introduced in ref 42.

RESULTS AND DISCUSSION

Single Mutants. Before starting with a systematic analysis including all nonconserved residues, we consider mutations for which experimental absorption shifts have been measured. Even before crystal structures of Rh were available, Lin et al.[6] investigated the effect of point mutations. They selected 12 residues that are nonconserved in HB, guided by three criteria, which are proximity to retinal, change in polarity, and change in polarizability. The first one was applied using a simple secondary structure model. On the basis of the X-ray structure, we consider all 10 of these residues that are not surface exposed (see Table 1). As expected, the remaining two (P107R and T108H) show negligible shifts (<0.01 eV) in the mutation experiment. The structural effects of these 10 mutations are described in the Supporting Information.

Table 1. Experimental and Calculated Shifts in Excitation Energy $\Delta\Delta E_{S1\leftarrow S0}$ (SORCI with CHARMM Charges, eV) and Minimal Distance to Retinal (Å)

mutant	exptl[6]	calcd	distance	helix
M86L	–	0.00	6.9	2
V87C	0.01	0.02	10.2	2
G90S	0.06	0.05[a]	6.3 (2.7[b])	2
A117G	0.02	−0.01	**2.8** (**2.3**[b])	3
E122L[c]	0.03	−0.02	**2.3**	3
A124T	0.02	0.03	5.6	3
W265Y	0.08	0.06	**2.1**	6
A292S	0.05	0.04	3.0	7
A295S_a	0.03	−0.01	**2.8**	7
A295S_b[d]	dto.	0.05		
A295S_c[d]	dto.	−0.06		
A299C	0.01	0.00	9.1 (7.8[b])	7
sum	0.31	0.16		

[a]Including Ser90 in the QM region (QM5_90) gives the same shift (0.05 eV). [b]Minimal distance to Wat2b. [c]Glu122 is protonated in WT Rh. Otherwise mutation to leucine would produce a shift of ≈0.6 eV.[39] [d]The mutant structure A295S_b is 1 kcal/mol higher in energy than A295S_a. A295S_c is 0.2 kcal/mol lower in energy.

Calculated shifts show good agreement with experiment for all but the three mutations that have large sterical effects and, at the same time, are close to retinal: A117G, E122L, and A295S. Structural changes involving helical movements or larger movements in side chain orientation are hard to find with our QM/MM MD simulations because of the short simulation time scales (ns). Also new water molecules and their effect on the structure are difficult to evaluate.

In the W265Y mutant structure, we added one water molecule (Wat45) to fill the space left by the larger Trp side chain. In MD simulations, this water forms stable hydrogen bonds to Tyr265 and the backbone oxygen of Ala117.

For A295S, we find three structures with energies within 1 kcal/mol, which yield quite different shifts. The structure highest

dx.doi.org/10.1021/jp2086472 | J. Phys. Chem. B 2012, 116, 3313−3321

in energy (A295S_b) produces a shift in good agreement with experiment (see Table 1) but rapidly converts into structure A295S_a during MD simulations. The shift of A295S_a is still reconcilable with experiment, whereas that of the lowest energy structure (A295S_c) is not. We tried to introduce a new water molecule close to Ser295, but in MD simulation no stable structure was found. Note that the main difference between A295S_a and A295S_b is the Ser295 hydrogen bond to the backbone of Ala292 and, respectively, Pro291 (see Supporting Information). The total energy differences are smaller than the accuracy of the classical force field used for modeling. Therefore, the A295_b orientation is possibly the most appropriate choice for the 10fold mutant, leading to the best agreement with experimental excitation energies. Nevertheless, we employed A295S_a as the starting point for the modeling of the multiple mutations, but this issue will be discussed in more detail below. Details of the structures of the ten single mutants are given in the Supporting Information.

Multiple Mutants. Lin et al.[6] also produced multiple mutants combining the mutations that are located on the same helix. These are called h2 (86, 90), h2′ (86, 87, 90), h3 (117, 122, 124), and h7 (292, 295, 299). The W265Y single mutation can also be called h6. We modeled all of these and also the combinations shown in Table 2. All multiple mutants that imply the W265Y mutation were modeled with the additional water molecule Wat45. Mutants which have also the mutations in helix 2 have another added water molecule (Wat46) between Wat45 and Wat2b. These are h267, h267+117, h267+122, h267+124, 9fold, and 10fold. This water molecule is added for the following reasons: (1) There is a large cavity formed by the M86L and A117G mutations, which provides space for one water molecule. (2) This water molecule is stable in MD simulations. (3) The absorption shift would be much smaller without this water molecule (e.g., only 0.04 eV for the h267 mutant). We tested adding a third water molecule in the cavity between Wat45, Wat46, and Ser295 in the 9fold and 10fold mutants, but this does not result in a stable configuration in MD simulations. In the energetically lowest configuration, the shift in excitation energy is similar to the one with only two added water molecules.

Table 2. Experimental and Calculated (SORCI) Shifts in Excitation Energy $\Delta\Delta E_{S1\leftarrow S0}$ (eV) of Multiple Mutants[a]

mutant	exptl[6]	calcd
h2	0.07	0.03
h2′	0.06	0.04
h3	0.06	0.03
h7	0.08	0.04
h27	0.13	0.05
h36	0.15	0.13
h237	0.14	0.09
h267	0.27	0.15
h267 + 117	0.27	0.17
h267 + 122	0.33	0.15
h267 + 124	0.20	0.17
9fold	0.35	0.21
10fold	0.36	0.22

[a]h27, e.g., refers to the 5-fold mutant that combines all single mutations on helices 2 and 7. "9fold" refers to h2367 and "10fold" to h2′367.

Many of the calculated shifts are significantly smaller than the experimental ones. Note, however, that a large portion of the computational error occurs for helices h3 and h7. This can be traced back to the errors of the single mutants of residues 117, 122, and 295; that is, again, the exact orientation of Ser295 might be essential for a better agreement with experiment. Both experiment and our theoretical model predict shifts of the 9fold and 10fold mutants that are super additive, indicating collaborative effects; e.g., the complex counterion is changed due to the new water Wat46, and Ser90 is differently oriented than in the G90S single mutant. The experimental (theoretical) shift from h27 to h267 is 0.14 (0.10) eV, but the shift in excitation energy of the W265Y single mutant is only 0.08 (0.06) eV, respectively.

Search for Further Essential Mutations. To identify further nonconserved amino acids that contribute to the shift, we first calculate the electrostatic contribution of each amino acid to the opsin shift in WT Rh (perturbation analysis). Then we consider additional amino acids that are nonconserved and close to the chromophore. For both selections, we model single and multiple mutants.

Table 3 shows the results of the perturbation analysis and lists all amino acids with an electrostatic effect $|ES^{\mathrm{WT\ Rh}}(I)| \geq 0.004$ eV.

Table 3. Results of the Perturbation Analysis (Residues with an Electrostatic Effect $|ES^{\mathrm{WT\ Rh}}(I)| \geq 0.004$ eV)[a]

residue	HB[b]	$ES^{\mathrm{WT\ Rh}}(I)$	residue	HB[b]	$ES^{\mathrm{WT\ Rh}}(I)$
Cys185		−0.004	Trp126		0.004
Tyr301		−0.005	Tyr206	Phe	0.004
Gln184		−0.005	**Glu122**	**Leu**	0.004
His100[c]	Asn	−0.005	Thr92	Phe	0.004
His152		−0.005	Ser127		0.005
Met207	Leu	−0.005	Thr289		0.005
Asn55		−0.006	Phe261		0.005
Thr93	Pro	−0.006	Ser98		0.007
Thr97	Ala	−0.007	Met44		0.009
Asn111	Ala	−0.007	Ser298	Ala	0.010
Thr178	Phe	−0.008	His211	Cys	0.015
Cys167	Val	−0.009	Phe293		0.019
Thr297	Ser	−0.011	Glu181		0.064
Tyr43	Phe	−0.018			
Tyr268		−0.022			
Trp265	**Tyr**	−0.024			
Tyr191	Trp	−0.025			
Ser186		−0.031			
Thr118		−0.043			

[a]Mutations already included in the 10-fold mutant are given in bold. [b]If the residue is nonconserved, its counterpart in HB is given. [c]His100 is located more than 16 Å away from the PSB at the outer surface of WT Rh and therefore was not modeled.

Only two of the 16 nonconserved residues in this list were included in the study of Lin et al.[6] (E122L and W265Y). Glu113 and Thr94 were not investigated in the perturbation analysis because they are part of the QM4 region. The T94V mutation is clearly important and will be considered, too. The H100N mutation will not be considered, as it is located more than 16 Å away from the PSB and at the outer surface of WT Rh. This makes 14 new mutations that will be considered in the following.

Table 4 shows the shifts in excitation energy of the 14 new single mutations in the perturbation analysis and from the

dx.doi.org/10.1021/jp2086472 | J. Phys. Chem. B 2012, 116, 3313−3321

Table 4. Shifts in Excitation Energy $\Delta\Delta E_{S1\leftarrow S0}$ of the 14 New Residues Selected in the Perturbation Analysis (in eV)[a]

	perturbation[b]	mutation[c]	mutation[c]
	OM2/MRCI	OM2/MRCI	SORCI
Y43F	0.018	0.03	0.02
T92F	−0.004	0.01	0.01
T93P	0.006	0.04	0.03
T94V	–	0.04	0.08
T97A	0.007	0.01	0.01
N111A	0.007	0.02	0.03
C167V	0.009	0.02	0.04
Y178F	0.008	0.02	0.01
Y191W	0.025	0.07	0.06
Y206F	−0.004	−0.01	−0.01
M207L	0.005	0.02	0.01
H211C	−0.015	−0.04	−0.04
T297S	0.011	0.00	−0.01
S298A	−0.004	−0.02	−0.02
sum	0.089	0.21	0.25

[a]Note: rounding after summation. [b]Shift in excitation $\Delta\Delta E_{S1\leftarrow S0}$ (WT Rh−WT Rh w/o residue I) is equal to $-ES^{WT\ Rh}(I)$. Without structure relaxation. [c]Single mutant with structure relaxation.

relaxed mutant structures. Some of the shifts of the single mutants are clearly different from the shift in the perturbation analysis (regardless of the QM method) because the mutations introduce new polar groups (Y191W, T297S) or have a structural effect on other residues. The sum of the shifts of the 14 single mutants is very large (+0.25 eV). This shows that some very important mutations were not included in the search of Lin et al.[6] A 24fold mutant was built that consists of the ten mutations in the 10fold mutant and the 14 new mutations.

On the structural level, the 24fold mutant shows cooperative effects; i.e., the structure is not simply the overlay of the single mutants. Because of the S298A mutation, the HBN of Tyr265, Wat45, and Wat46 is slightly changed. Tyr265 forms a hydrogen bond to a water molecule that is part of the HBN around Asp83. The HBN in the 24fold mutant is slightly less stable than in the 9fold and 10fold mutants. After 200 ps of MD simulation, the HBN changes strongly, but no other stable configuration is found afterward. As shown in Table 5, the

Table 5. Shifts in SORCI Excitation Energy of Multiple Mutants (in eV)

	$\Delta\Delta E_{S1\leftarrow S0}$
9fold	0.21
10fold	0.22
24fold	0.36
24fold_b[a]	0.25
30fold	0.42
HB (exptl)	0.45

[a]24fold mutant with a third extra water and a strongly changed HBN of Tyr265, waters 44−47, Wat2b, and Ser90.

24fold mutant structure gives a shift in excitation energy of 0.36 eV, which is 0.14 eV larger than that of the 10fold mutant but smaller than the sum of single mutations (0.39 eV).

We built another structure for the 24fold mutant by adding a third water in the free space left by the S298A mutation. An instable configuration 24fold_b was found in MD simulations with a completely changed HBN of Tyr265, waters 45−47, Wat2b, and Ser90. The shift in excitation energy of 24fold_b (0.25 eV) is only 0.03 eV larger than that of the 10fold mutant. This is in contrast to the large shifts of the 14 single mutants and comes from the large structural changes in the HBN. Wat45 and Wat46 reorient their dipole moments. Instead of stabilizing the PSB excess charge in the ground state, like in the 10fold mutant, they destabilize it, which gives rise to a much lower excitation energy of the 24fold_b mutant. Because of this smaller shift in excitation energy and the smaller stability in MD simulations, we choose the 24fold mutant structure without the third extra water for further investigations. Table 5 shows the shifts in excitation energy for both 24fold mutant structures.

The search for mutations within 5 Å of retinal covers six of the 12 residues selected by Lin et al. and yields six more residues that are different in HB (Table 6). Individually, these

Table 6. Shifts in SORCI Excitation Energy of the Six Single Mutants (in eV)

	$\Delta\Delta E_{S1\leftarrow S0}$
L47V	−0.002
F91V	0.005
L125G	0.004
I189P	−0.003
L266V	−0.003
V300I	0.000

single mutants give very small shifts in excitation energy that essentially cancel (see Table 6). Adding all six mutations to the 24fold mutant, we obtain the 30fold mutant, which has the surprisingly large shift of 0.42 eV, even 0.06 eV larger than that of the 24fold mutant (see Table 5).

To investigate the large difference between the 24fold and 30fold mutant, we built three more structures, 28fold (≙30fold w/o L125G, I189P), 28fold+125 (≙30fold w/o I189P), and 28fold+189 (≙30fold w/o L125G). The 28fold mutant has still the same excitation energy as the 24fold mutant. The two different 29fold mutants, in contrast, absorb ≈0.03 eV higher in energy and in combination produce the 0.06 eV difference to the 30fold mutant.

The reason for these surprisingly large shifts, which are expected neither from the perturbation analysis nor from the single mutants (L125G and I189P), can be found in a displacement of retinal in the direction of the β-ionone ring (≈0.5 Å) due to steric effects of the L125G and I189P mutations. The inflexible Pro189 "pushes" against the methyl group at C_9, and the small Gly125 leaves space for the β-ionone ring to move in this direction (see Figure S-18 in the Supporting Information). In Rh, the negatively charged Glu181 is located close to the center of retinal and does not change its position with respect to the protein matrix. In the 30fold mutant, Glu181 is therefore closer to the PSB and further away from the β-ionone ring, which results in a larger hypsochromic shift. Table 7 shows the movements and the shifts in excitation energy.

Water molecules and structural details in the HBN in the vicinity of retinal have a significant impact on the excitation energy; therefore, these have been carefully examined in most modeling studies of rhodopsins. It is particularly interesting that our 10fold mutant model does not reproduce the experimental shift, possibly due to problems in modeling the HBN, as discussed above. The structural changes that occur in the HBN

dx.doi.org/10.1021/jp2086472 | J. Phys. Chem. B 2012, 116, 3313−3321

Table 7. Shifts in the SORCI Excitation Energy of Multiple Mutants (eV) and Distances from $O_{\varepsilon 1}$ of Glu181 to N_{16} (PSB) and C_6 (β-Ionone Ring) (Å)

		Glu181 $O_{\varepsilon 1}$ to	
	$\Delta\Delta E_{S1\leftarrow S0}$	N_{16}	C_6
24fold	0.36	7.3	9.0
28fold	0.35	7.3	9.0
28fold+125	0.39	7.2	9.1
28fold+189	0.40	7.2	9.1
30fold	0.42	7.1	9.2

of the 24fold and 30fold models then lead to a blue shift that is close to the experimental one for HB. Also in the 24fold mutant, we tested the alternative orientations of the hydrogen bond of Ser295, which was problematic in the 10fold mutant. We found that in the 24fold structure they all relax into the same configuration (referred to as A295S_a above) already during geometry optimization. Therefore, the shift predicted for the 24fold mutant might be more realistic than that of the 10fold mutant, although experimental data would be necessary to confirm this point.

Our 30fold mutant includes four residues from Lin's original selection that are not covered by the two selection criteria, (1) perturbation analysis and (2) distance constraint. Only one of these mutations (A124T) causes structural changes close to the binding pocket (6−8 Å from retinal). A refined selection criterion might therefore use larger distance constraints for mutations that change polarity or size of the residue. In the Supporting Information, we describe the structural aspects of all single mutations and the cooperative effects playing a role for multiple mutant structures.

Decomposition of the Blue Shift. The sum of shifts of single mutations is not equal to the shift of the multiple mutants. This was shown to be because of cooperativity of some mutations that interact directly or via a HBN and cause larger-scale structural changes. In this section, we elucidate the mechanisms behind the blue shift of the 30fold mutant. First we compare the electrostatic contributions of individual amino acids before and after structural changes. Then we discuss the role of the complex counterion and steric effects on the chromophore geometry.

To evaluate the combined effect of mutation and structural changes for each residue, we again use a perturbation analysis. Here we compare the electrostatic effect $ES^X(I)$ of each residue I in WT Rh and in the 30fold mutant

$$\Delta ES^{30\text{-fold}-\text{WT Rh}}(I) = ES^{30\text{-fold}}(I) - ES^{\text{WT Rh}}(I) \quad (2)$$

The sum of all electrostatic shifts amounts to 0.36 eV (Table 8), of which the mutated residues account for 0.24 eV. The largest shifts come from the A292S and Y191W mutations and from the two newly introduced water molecules 45 and 46. Interestingly, also conserved residues and water molecules contribute substantially to the electrostatic shift, 0.12 eV in total. This can be attributed to polar groups that are reorientated (Ser186 and Wat2a due to A292S, Wat6 due to E122L and H211C, or Wat14 due to A124T mutations) or to changed distances to retinal (Met44 due to T94V, Glu113 and Wat2b due to T94V and G90S, or Tyr268 due to the Y191W mutation). The electrostatic shifts of Thr118, Glu181, and Phe293 are due to distance changes to retinal as a consequence

Table 8. Electrostatic Effects in WT Rh and the 30Fold Mutant and Electrostatic Shifts of Mutated Residues (Calculated with OM2/MRCI in eV)[a]

residue	$ES^{\text{WT Rh}}$	$ES^{30\text{fold}}$	$\Delta ES^{30\text{fold}-\text{WT Rh}}$	mutation
90	–[b]	−0.02	−0.02	Gly→Ser
122	0.01	0.00	−0.01	Glu→Leu
124	0.00	0.01	0.01	Ala→Thr
292	0.00	0.05	0.05	Ala→Ser
94[c]	−0.02	0.00	0.02	Thr→Val
191	−0.03	0.00	0.03	Tyr→Trp
211	0.01	0.00	−0.01	His→Cys
Wat45	–[d]	0.06	0.06	new water
Wat46	–[d]	0.03	0.03	new water
Sum of all mutated residues = 0.24				
44	0.01	0.00	−0.01	Met
113[e]	0.46	0.65	0.10	Glu
118	−0.05	−0.02	0.02	Thr
181	0.06	0.05	−0.02	Glu
186	−0.03	−0.05	−0.02	Ser
268	−0.02	−0.01	0.02	Tyr
293	0.02	0.01	−0.01	Phe
6	−0.01	−0.01	0.01	water
Wat2a	0.05	0.06	0.01	water
14	−0.01	0.01	0.01	water
Wat2b[c]	−0.01	−0.02	−0.01	water
Sum of all conserved residues = 0.12				

[a]Note: rounding after summation. [b]For a glycine residue, no electrostatic effect $ES^X(I)$ can be calculated. [c]Values are from a QM2 calculation because residue 94 is part of the QM4 region. [d]Wat45 and 46 are newly introduced in the 30fold mutant. [e]Values are from a QM1 calculation because residue 113 is part of the QM4 and QM2 region.

of collaborative effects rather than individual mutations. All other residues produce electrostatic shifts smaller than 0.02 eV.

In previous studies on spectral tuning of rhodopsins, the opsin shift or the shift between different proteins was decomposed into contributions from the chromophore geometry, the structure of the complex counterion, and the protein electrostatics. We obtain the same partitioning for the 0.42 eV blue shift of the 30fold mutant wrt WT Rh, based on SORCI calculations with different QM regions (Table 9).

Table 9. Decomposition of the Shift Between WT Rh and the 30-Fold Mutant (SORCI Results, eV)[a,b]

	$\Delta\Delta E_{\text{vacuo}}^{30\text{-fold}-\text{Rh}}$	$\Delta ES^{30\text{-fold}-\text{Rh}}$	$\Delta\Delta E_{\text{protein}}^{30\text{-fold}-\text{Rh}}$
QM4	0.11	0.31	0.42
QM2	0.13	0.28	0.42
QM1	0.02	0.35	0.37

[a]Note: rounding after summation. [b]$\Delta ES^{30\text{-fold}-\text{Rh}}$ is the difference between the full QM/MM shift $\Delta\Delta E_{\text{protein}}^{30\text{-fold}-\text{Rh}}$ and the QM shift in vacuo (omitting the point charges) $\Delta\Delta E_{\text{vacuo}}^{30\text{-fold}-\text{Rh}}$.

The first component can be associated with the shift in excitation energy of the bare chromophore (QM1) without point charges and amounts to 0.02 eV (5%). The main difference in chromophore geometry is an increased bond-length alternation (BLA). As a direct consequence, the dihedral distortion of single (double) bonds in the conjugated chain is increased (decreased) by 3.1° (2.4°). As shown in Table 9, the BLA responds to the electric field along the conjugated chain

dx.doi.org/10.1021/jp2086472 | J. Phys. Chem. B 2012, 116, 3313−3321

and is strongly correlated with the excitation energy. Other geometric parameters that affect the excitation energy are basically unchanged. This includes the distance between the PSB nitrogen and C6, which is a measure for the global bending and twist of the conjugated chain, as well as the dihedral of the C6−C7 bond as a measure for the coplanarity of the β-ionone ring (see Supporting Information).

The complex counterion is essentially contained in the QM4 region. Hence the second component can be obtained from the difference of QM4 and QM1 calculations in the gas phase (first column in Table 9) and amounts to 0.09 eV (21%). As noted above, the structure of the counterion is mostly affected by the T94V and G90S mutations, which reduce the separation between Glu113 and the PSB.

The largest component is the protein electrostatic effect, i.e., the difference between the shifts of the in vacuo and QM/MM calculations using the QM4 region. It amounts to 0.31 eV (74%) and has been analyzed above.

Correlation of BLA and Excitation Energy. Bond-length alternation (BLA) is the difference between the average length of the five single and the six double bonds in retinal's π-system. For WT Rh, the BLA is 0.067 Å. For the 30fold mutant, it is increased to 0.079 Å. The BLA is strongly correlated to the C=C stretch frequency $\nu_{C=C}$, which can be measured with Raman spectroscopy, and to the UV−vis absorption $\Delta E_{S1\leftarrow S0}$. The linear correlation of $\nu_{C=C}$/BLA and $\Delta E_{S1\leftarrow S0}$ was shown by Kochendoerfer et al.[5,7] experimentally and by our group computationally.[41]

As shown in Figure 1, the single and multiple mutants in this work show a strong linear dependence of excitation energy and

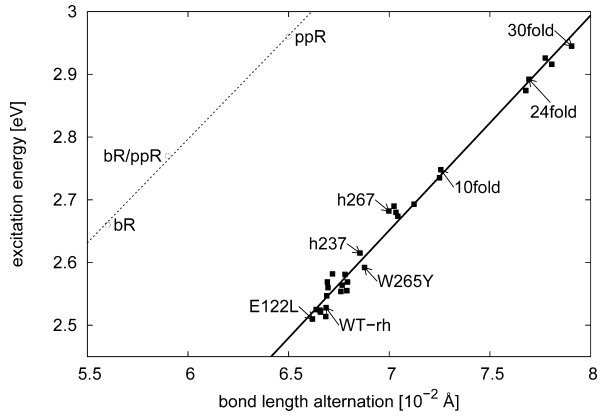

Figure 1. Linear correlation of excitation energy and bond length alternation (■, this work; ○, Hoffmann et al.[41]).

the BLA, with the same slope as found for archaeal rhodopsins[41] (0.34 eV/0.01 Å). The offset is expected to be because of the different retinal conformations (all-*trans* in bR and ppR and 11-*cis* in Rh and HB) and different sizes of the QM region.

■ CONCLUSIONS

In this work, we investigated the structural origin of the 0.45 eV shift in the UV−vis absorption maximum between the Rh and HB pigments. In principle, one can follow two different approaches. (a) The first is to use homology modeling. Here, the major difficulties are to consider the possible rotamer states and to account for missing water molecules. Trabanino et al.[8] constructed a homology model and optimized the side chain rotamers based on the potential energy. Fujimoto et al.[9−11] and Altun et al.[12] used the homology model of Stenkamp et al.[13] importing the water molecules from the Rh X-ray structure. Note that these studies did not invoke large MD simulations to equilibrate the structure and allow for sufficient solvation. (b) The second approach makes use of the fact that color tuning is dominated by interactions in the vicinity of the chromophore;[41,49,50] i.e., most of the color shift can be realized by replacing amino acids in the binding pocket. Therefore, one can construct a HB model by replacing amino acids in the binding pocket of Rh by those present in HB. This allows us to investigate the different factors responsible for the color shift in detail. Compared with the homology model, the reduced number of mutations facilitates the rigorous search for the correct rotamer states and missing water molecules. Starting from the latest Rh X-ray structure of Okada et al.,[42] we built structural models of single and multiple mutants of Rh and performed nanosecond QM/MM MD simulations. The multiple mutants are constructed stepwise and are carefully equilibrated to verify the correct rotamers. We considered 10 residues that were experimentally studied and selected 20 further residues using two criteria, their electrostatic influence on the excitation energy and their proximity to the chromophore (within 5 Å). The resulting 30fold mutant is predicted to absorb at 2.89 eV and achieves a blue shift of 0.42 eV compared to Rh (2.47 eV), which is 93% of the experimental shift of HB.

Both approaches involve certain difficulties that are related to the lack of sufficient sampling. The relevant time scales could possibly be reached using classical MD simulations and enhanced sampling techniques,[15] but a convergence would still not be guaranteed when larger structural changes are involved. Moreover, classical force fields are not able to describe the hydrogen-bonded structure around PSB. All MD simulations performed so far led to a collapse of the retinal binding pocket.[15] Therefore, QM/MM MD seems to be crucial, unless a polarized force field is used. QM/MM simulations, even using approximate QM methods like SCC-DFTB, are limited to much shorter (nanosecond) time scales, as performed in this study. Sufficient equilibration in the nanosecond regime is feasible for mutations of individual or uncorrelated residues when the substituted side chain is of similar size, differing only in charge or dipole moment.[41] Problems arise when (1) various rotamer states arise. Here, the energy differences can be so small (below 1 kcal/mol) that the accuracy of the force field and QM methods is not sufficient to decide on the right rotamer. Nevertheless, these different rotamer states can lead to drastic changes in excitation energy, as is the case for our 10fold mutant model. (2) When the size of the amino acid changes significantly, voids for additional water molecules may occur. The latter can cause significant shifts in excitation energy and therefore should not be neglected. However, their exact placement is again a difficult issue. Sophisticated methods like grand canonical simulations rely on the force field energetics, which may be problematic in strongly hydrogen-bonded systems, as discussed above. Therefore, we based our assessment on QM/MM MD simulations, which are clearly limited in simulation time but provide a stable retinal binding pocket. (3) Third, amino acid substitutions in the binding pocket can lead to structural changes that affect the retinal conformation. Of particular importance are changes in the retinal dihedral angles, which can lead to substantial shifts in excitation energy, e.g., at the 6-s-*cis* bond, as discussed recently.[49]

dx.doi.org/10.1021/jp2086472 | J. Phys. Chem. B 2012, 116, 3313−3321

Concerning point (3), the situation remains unclear. Trabanino et al.[8] did not report any change of the 6-s-*cis* torsional angle with respect to the green and red pigments. Using the homology model of Stenkamp,[13] Fujimoto et al.[9] found no large difference in the retinal conformation after QM/MM optimization. In a latter paper, using the same computational approach, a twist of the 6-s-*cis* bond has been reported.[10,11] Note that Trabanino et al.[8] performed MD simulations to equilibrate the structures, which may lead to a relaxation of the PSB that is not obtained from a simple geometry optimization. On the other hand, a twist of this bond could be expected from theoretical reasoning.[49,50] In our 30-fold model, we observe a larger shift of retinal due to mutations in the binding pocked (L125G and I189P). We do not find any additional twist in the 6-s-*cis* moiety but cannot exclude that such a twist would occur in longer time scale MD simulations.

We have shown that a simple perturbation analysis that measures the shift in excitation energy induced by the partial charges of the individual residues represents a useful heuristic tool. In most cases, however, it is not sufficient to predict the actual effect of mutation. Structural relaxation must be accounted for, even in the case of single mutants. Our relaxed mutant models reproduce nicely the experimental data, except for the residues 117, 122, and 295, which we attribute to the applied harmonic constraints, which prevent large-scale distortions of the protein, such as helix movement. Our multiple mutant models demonstrate various tuning mechanisms: (i) direct local modification of the electrostatic field (Y191W, 0.03 eV), (ii) mutations that act indirectly causing structural changes (T94V and G90S modify the geometry of the complex counterion, 0.10 eV), (iii) mutations that contribute only collectively combined with other mutations (steric effects of L125G and I189P, 0.06 eV), conserved as well as nonconserved residues that passively contribute in the course of structural changes (Glu113, 0.10 eV; A292S, 0.05 eV), and finally (iv) water molecules that fill hydrophilic cavities created by mutations (W265Y, 0.06 eV; M86L, A117G 0.03 eV). We observe that collaborative effects can enhance as well as reduce the shift. In agreement with experiment, we find the shift of the 10fold mutant to be larger than the sum of single mutant shifts. The opposite applies to the 24fold mutant, where structural changes reduce the shift, whereas in the 30fold mutant collaborative structural changes produce a sizable shift of 0.06 eV.

In difference to studies based on the homology model,[11,12] we find only a minor contribution to the blue shift of our 30-fold model arising from the chromophore geometry (+0.02 eV, or 5%), which is due to the increased BLA. The geometrical changes in the complex counterion, mainly due to T94V and G90S mutations, cause an additional shift of +0.10 eV. The remainder of the protein matrix causes a further shift of +0.30 eV (71%).

Finally, we have shown that for our mutants the BLA of retinal's conjugated π-system is linearly correlated with the excitation energy, in agreement with previous theoretical studies and consistent with the experimentally observed correlation between excitation energy and the vibrational frequencies of IR C=C and C=N stretch bands. Note that changes in the BLA are caused by the protein electrostatic field, i.e., the potential difference between the two ends of the conjugated chain, but the associated shift in excitation energy is merely a small fraction of the total shift, when including the electrostatic potential in the QM Hamiltonian (see also refs 41 and 51).

■ ASSOCIATED CONTENT

Supporting Information

Provided are additional data on charge transfer, MM polarization, retinal geometry, details of all mutant models, and electrostatic shifts. This material is available free of charge via the Internet at http://pubs.acs.org.

■ AUTHOR INFORMATION

Corresponding Author

*E-mail: marcus.elstner@kit.edu.

Notes

The authors declare no competing financial interest.

■ ACKNOWLEDGMENTS

This work was supported by the Deutsche Forschungsgemeinschaft via Forschergruppe 490 and SFB 498 and by the Spanish MICINN "Juan de la Cierva" program.

■ REFERENCES

(1) Kandori, H.; Shichida, Y.; Yoshizawa, T. *Biochemistry (Moscow)* **2001**, *66*, 1197−1209.
(2) Oprian, D. D. *Biochemistry* **1991**, *30*, 11367−11372.
(3) Merbs, S. L.; Nathans, J. *Nature* **1992**, *356*, 433−435.
(4) Fasick, J. I.; Lee, N.; Oprian, D. D. *Biochemistry* **1999**, *38*, 11593−11596.
(5) Kochendoerfer, G. G.; Lin, S. W.; Sakmar, T. P.; Mathies, R. A. *Trends Biochem. Sci.* **1999**, *24*, 300−305.
(6) Lin, S. W.; Kochendoerfer, G. G.; Carroll, K. S.; Wang, D.; Mathies, R. A.; Sakmar, T. P. *J. Biol. Chem.* **1998**, *273*, 24583−24591.
(7) Kochendoerfer, G. G.; Wang, Z.; Oprian, D. D.; Mathies, R. A. *Biochemistry* **1997**, *36*, 6577−6587.
(8) Trabanino, R. J.; Vaidehi, N.; Goddard, W. A. III *J. Phys. Chem. B* **2006**, *110*, 17230−17239.
(9) Fujimoto, K.; Hasegawa, J. .; Hayashi, S.; Nakatsuji, H. *Chem. Phys. Lett.* **2006**, *432*, 252−256.
(10) Fujimoto, K.; ya Hasegawa, J.; Nakatsuji, H. *Chem. Phys. Lett.* **2008**, *462*, 318−320.
(11) Fujimoto, K.; Hasegawa, J. Y.; Nakatsuji, H. *Bull. Chem. Soc. Jpn.* **2009**, *82*, 1140−1148.
(12) Altun, A.; Yokoyama, S.; Morokuma, K. *J. Phys. Chem. A* **2009**, *113*, 11685−11692.
(13) Stenkamp, R. E.; Filipek, S.; Driessen, C. A. G. G.; Teller, D. C.; Palczewski, K. *Biochim. Biophys. Acta, Biomembr.* **2002**, *1565*, 168−182.
(14) Teller, D. C.; Okada, T.; Behnke, C. A.; Palczewski, K.; Stenkamp, R. E. *Biochemistry* **2001**, *40*, 7761−7772.
(15) Babitzki, G.; Denschlag, R.; Tavan, P. *J. Phys. Chem. B* **2009**, *113*, 10483−10495.
(16) Duan, L. L. *J. Chem. Phys.* **2009**, *130*, 115102.
(17) Tong, Y.; Ji, C. G.; Mei, Y.; Zhang, J. Z. H. *J. Am. Chem. Soc.* **2009**, *131*, 8636−8641.
(18) Warshel, A.; Levitt, M. *J. Mol. Biol.* **1976**, *103*, 227−249.
(19) Field, M. J.; Bash, P. A.; Karplus, M. *J. Comput. Chem.* **1990**, *11*, 700−733.
(20) Gao, J. *Acc. Chem. Res.* **1996**, *29*, 298−305.
(21) Senn, H.; Thiel, W. *Top. Curr. Chem.* **2007**, *268*, 173−290.
(22) MacKerell, A.; et al. *J. Phys. Chem. B* **1998**, *102*, 3586−3616.
(23) Elstner, M.; Porezag, D.; Jungnickel, G.; Elsner, J.; Haugk, M.; Frauenheim, T.; Suhai, S.; Seifert, G. *Phys. Rev. B* **1998**, *58*, 7260−7268.
(24) Wanko, M.; Hoffmann, M.; Strodel, P.; Koslowski, A.; Thiel, W.; Neese, F.; Frauenheim, T.; Elstner, M. *J. Phys. Chem. B* **2005**, *109*, 3606−3615.
(25) Cui, Q.; Elstner, M.; Kaxiras, E.; Frauenheim, T.; Karplus, M. *J. Phys. Chem. B* **2001**, *105*, 569−585.
(26) Elstner, M.; Cui, Q. In *Solvation Effects. Methods and Applications*; Canuto, S., Ed.; Springer Series: Challenges and

Advances in Computational Chemistry and Physics; Springer: New York, 2008; Chapter Combined QM/MM methods for the simulation of condensed phase processes using an approximate DFT approach.
(27) Cui, Q.; Elstner, M. In *Multiscale Quantum Models for Biocatalysis: Modern Techniques and Applications*; Lee, T., York, D., Eds.; Springer: New York, 2008; Chapter Multi-Scale QM/MM methods with Self-Consistent-Charge Density-Functional-Tight-Binding (SCC-DFTB).
(28) Yang, Y.; Yu, H.; York, D.; Cui, Q.; Elstner, M. *J. Phys. Chem. A* **2007**, *111*, 10861−10873.
(29) König, P.; Hoffmann, M.; Frauenheim, T.; Cui, Q. *J. Phys. Chem. B* **2005**, *109*, 9082−9095.
(30) Nose, S. *J. Chem. Phys.* **1984**, *81*, 511−519.
(31) Hoover, W. G. *Phys. Rev. A* **1985**, *31*, 1695−1697.
(32) Thiel, W. *MNDO99*, version 6.1; Max-Planck-Institut für Kohlenforschung: Mülheim an der Ruhr, Germany, 2006.
(33) Weber, W.; Thiel, W. *Theor. Chem. Acc.* **2000**, *103*, 495−506.
(34) Neese, F. *J. Chem. Phys.* **2003**, *119*, 9428−9443.
(35) Neese, F. *ORCA - An ab initio, density functional and semiempirical program package*; Version 2.4 - Revision 41; Max Planck Institut fuer Strahlenchemie: Muelheim, Germany, 2005.
(36) Schäfer, A.; Horn, H.; Ahlrichs, R. *J. Chem. Phys.* **1992**, *97*, 2571−2577.
(37) Wanko, M.; Hoffmann, M.; Frauenheim, T.; Elstner, M. *J. Phys. Chem. B* **2008**, *112*, 11462−11467.
(38) Wanko, M.; Hoffmann, M.; Frähmcke, J.; Frauenheim, T.; Elstner, M. *J. Phys. Chem. B* **2008**, *112*, 11468−11478.
(39) Frähmcke, J. S.; Wanko, M.; Phatak, P.; Mroginski, M. A.; Elstner, M. *J. Phys. Chem. B* **2010**, *114*, 11338−11352.
(40) Phatak, P.; Frähmcke, J. S.; Wanko, M.; Hoffmann, M.; Strodel, P.; Smith, J. C.; Suhái, S.; Bondar, A. N.; Elstner, M. *J. Am. Chem. Soc.* **2009**, *131*, 7064−7078.
(41) Hoffmann, M.; Wanko, M.; Strodel, P.; König, P. H.; Frauenheim, T.; Schulten, K.; Thiel, W.; Tajkhorshid, E.; Elstner, M. *J. Am. Chem. Soc.* **2006**, *128*, 10808−10818.
(42) Okada, T.; Sugihara, M.; Bondar, A. .; Elstner, M.; Entel, P.; Buss, V. *J. Mol. Biol.* **2004**, *342*, 571−583.
(43) Palczewski, K.; Kumasaka, T.; Hori, T.; Behnke, C. A.; Motoshima, H.; Fox, B. A.; Le Trong, I.; Teller, D. C.; Okada, T.; Stenkamp, R. E.; et al. *Science* **2000**, *289*, 739−745.
(44) Okada, T.; Fujiyoshi, Y.; Silow, M.; Navarro, J.; Landau, E. M.; Shichida, Y. *Proc. Natl. Acad. Sci. U.S.A.* **2002**, *99*, 5982−5987.
(45) Li, J.; Edwards, P. C.; Burghammer, M.; Villa, C.; Schertler, G. F. *J. Mol. Biol.* **2004**, *343*, 1409−1438.
(46) Standfuss, J.; Xie, G.; Edwards, P. C.; Burghammer, M.; Oprian, D. D.; Schertler, G. F. X. *J. Mol. Biol.* **2007**, *372*, 1179−1188.
(47) Lüdeke, S.; Beck, R.; Yan, E. C. Y.; Sakmar, T. P.; Siebert, F.; Vogel, R. *J. Mol. Biol.* **2005**, *353*, 345−356.
(48) Dinner, A. R.; Lopez, X.; Karplus, M. *Theor. Chem. Acc.* **2003**, *109*, 118−124.
(49) Tomasello, G.; Olaso-Gonzales, G.; Altoe, P.; Stenta, M.; Serrano-Andres, L.; Merchan, M.; Orlandi, G.; Bottoni, A.; Garavelli, M. *J. Am. Chem. Soc.* **2009**, *131*, 5172−5186.
(50) Altoe, P.; Cembran, A.; Olivucci, M.; Garavelli, M. *Proc. Natl. Acad. Sci. U.S.A.* **2010**, *107*, 20172−20177.
(51) Hufen, J.; Sugihara, M.; Buss, V. *J. Phys. Chem.* **2004**, *108*, 20419−20426.